Solar Energy 180 (2019) 243–256

Contents lists available at ScienceDirect

Solar Energy

journal homepage: www.elsevier.com/locate/solener

Numerical characterization of thermocline behaviour of combined sensible-latent heat storage tank using brick manganese rod structure impregnated with PCM capsules

N. Ahmed, K.E. Elfeky, Mumtaz A. Qaisrani, Q.W. Wang*

Key Laboratory of Thermo-Fluid Science and Engineering, MOE, Xi'an Jiaotong University, Xi'an, Shaanxi 710049, China

ARTICLE INFO

Keywords:
Thermal energy storage
Thermocline thickness
Phase change materials
Sensible-latent heat storage

ABSTRACT

Efficient medium temperature thermal energy storage (TES) can help to eliminate the imbalance between energy demand and supply. In this study the issue of thermal ratcheting in TES system is avoided by using structured sensible heat storage material. Another technical issue of temperature drops at the end of discharging cycles occurring in only sensible material filled TES is overcome to some extent by using phase change material (PCM) between sensible rod structure (SRS) providing stable fluid outlet temperature. A comprehensive transient numerical model is formulated by solving separate equations for heat transfer fluid and storage materials using energy balance method coupled with enthalpy technique to study the influence of phase change temperature in the PCM. The numerical model predicts thermal stratification behaviour and thermocline formation along the symmetry-axis. A detailed parametric analysis of the combined sensible-latent heat thermal energy storage is performed to investigate the effect of porosity variation, inlet velocity and feature size of sensible heat storage material on total energy utilization, effective discharging efficiency and effective discharging time using thermocline characterization. The results indicate that discharging efficiency of hybrid TES tank can be increased by using lower velocity of fluid at inlet, by decreasing porosity or by using reduced SRS feature size. The study offers suggestions for optimized design and governing parameters of a new type of combined sensible-latent heat TES configuration, while avoiding thermal ratcheting with stable fluid outlet temperature for an application specific process.

1. Introduction

To eliminate the imbalance between energy supply and demand is a tough challenge for researchers in the current global energy scenario (Kılkış et al., 2018). The contribution of TES units can be enhanced by taking the advantage of large-scale switching characteristics of thermal energy systems (Gasia et al., 2017). To extract maximum solar energy (Pelay et al., 2017) and entrap waste heat from industrial processes (Jiménez-Arreola et al., 2018) are considered as potential alternate energy resources. These energy resources find their medium temperature applications in hot water supply for industrial and domestic usage, greenhouse warming for agricultural purpose, space heating for commercial buildings etc. However, the intermittency and unpredictability of the energy sources make it vulnerable (Dincer and Rosen, 2002). In recent years, this lead researchers to focus their attention on new innovative TES systems and are considering it as an efficient method to make the energy resource sustainable and more efficient (Kılkış et al., 2018).

In a TES useful energy from the heat source is transferred to storage material as a change in its internal energy. It is stored as sensible heat, latent heat and thermochemical heat or it can be a combination of these (Gil et al., 2010). Both sensible and latent heat storage types have advantages and disadvantages. Although sensible heat thermal energy storage (SHTES) systems are well developed and simple, constituting cheap storage materials like brick manganese, concrete etc. But these are not much attractive because of low storage capacity per unit volume and temperature drops at the end of discharging cycles(Gasia et al., 2017). Whereas, latent heat thermal energy storage (LHTES) is comparatively more attractive because of high storage capacity per unit volume with small temperature swings(Abhiji et al., 2015). LHTES using phase change materials also offer some other advantages like small storage unit size and isothermal characteristics during charging and discharging cycles. However, these storage systems are not much in commercial use as SHTES systems because of low thermal conductivity, inconsistent thermo-physical properties under extended cycles, high

* Corresponding author.
E-mail address: wangqw@mail.xjtu.edu.cn (Q.W. Wang).

https://doi.org/10.1016/j.solener.2019.01.001
Received 10 May 2018; Received in revised form 11 December 2018; Accepted 1 January 2019

Nomenclature

U	superficial velocity, m/s
t_c	cutoff time, s
T	temperature, K
$T_{f,out}$	HTF temperature at outlet, K
T_{final}	final temperature of storage material, K
X	melt fraction of PCM
H_{PCM}	enthalpy of PCM, J/kg
h_0	overall heat transfer coefficient, W/m^2 K
h_v	volumetric heat transfer coefficient, W/m^3 K
Re	Reynolds number
Nu	Nusselt number
Pr	Prandtl number
A_s	surface area, m^2
Δx	size of control volume, m
η_{dis}	discharging efficiency
$Q_{initially}$	energy initially stored in tank, kJ
Q_f	energy of HTF, kJ
Q_{SRS}	energy of SRS, kJ

Greek characters

ρ	density, kg/m^3
ε	porosity
μ	viscosity, kg/m s
η	efficiency

Subscripts

f	fluid
SRS	sensible rod structure
PCM	phase change material

cost, poor heat transfer rates during charging and heat recovery cycles (Dincer and Rosen, 2002). The main reason can be attributed to the fact that the convective interaction of solid-liquid interface of PCM with HTF is reduced due to the increased thermal resistance of developing solid layer inside PCM (Elfeky et al., 2018). Thus causing poor heat transfer rate.

These issues with sensible and latent heat storages need to be technically resolved before they can be widely available for commercial use. The hybrid combination of sensible and latent heat storage materials can help to eliminate the issues experienced in SHTES and LHTES to some extent and combine the advantages of both systems (Pelay et al., 2017). The advantage of cheap naturally occurring material can be enjoyed more effectively by the use of PCM helping to improve the degradation of thermocline region at the outlet of storage tank. This results into prolonging effective discharging time (Mat et al., 2013).

In single tank storage systems, high heated region and low heated regions are separated by thermal gradient called thermocline. One tank type TES systems are 20–37% more cheap than two tank type TES systems (Libby, 2010). Moreover, thermocline characteristics of single tank TES system make it more favorable to use low-cost solid storage material. Literature study reveals that packed bed was first modeled and analytically studied by Schumann (Schumann, 1929) and a large number of studies reported in the literature has focused on Schumann's model equations. A very useful review on different experimental and numerical studies using thermocline storage tanks for solar thermal was presented by Flueckiger et al (Flueckiger et al., 2013). After the evaluation of thermocline characteristics and performing thermal cycling tests, Sandia National Laboratories identified silica sand and quartzite rock as a potential low-cost solid storage material (Brosseau et al., 2005). Moreover, recently thermal stability of gneiss rock was investigated experimentally up to 1000 °C as the potential candidate for cheap sensible heat storage material (Jemmal et al., 2016). In most of the SHTES studies packed aggregate bed is typically used as storage material in thermocline storage tanks (Brosseau et al., 2005; Hänchen et al., 2011; Jemmal et al., 2016; Meier et al., 1991; Van Lew et al., 2011). However, this system experiences a critical technical issue of thermal ratcheting. Repeated thermal cycles during charging and discharging results into high lateral stresses on lower part of the tank walls due to the settlement of aggregate filler material caused by expanded tank volume (Flueckiger et al., 2012). Thermal ratcheting of storage tank walls caused by the use of packed bed storage material reduces life time of TES unit and its reliability. Therefore, the authors (Strasser and Selvam, 2014) proposed structured concrete design. The advantage of using structured solid material over aggregate filler is that it abolishes thermal ratcheting and for a given volume more thermal energy can be accommodated even at higher temperatures (Abarr et al., 2017).

The performance of single storage tank is derived by thermocline region formation. The filler materials in TES tank help to maintain thermal gradient for improved thermocline characteristics (Qin et al., 2012). The Passive TES systems filled with concrete as sensible heat storage material are usually embedded with tubular heat exchanger. This enables high heat transfer rates due to high thermal conductivity and increased contact area between them. However, the temperature may vary during discharging cycles. This issue can be overcome by using phase change materials but with lower heat exchange rates (Alva et al., 2017). Thermal performance and stratification behavior of single TES tank using PCMs were studied by many authors. The studies conducted by authors (Abhiji et al., 2015; Kumaresan et al., 2011; Singh et al., 2018) using DSCmeasurement suggest that D-Mannitol as the most suitable latent heat storage material for medium temperature applications. This is because it possesses large temperature difference of 405 K between its melting point and decomposition temperature.

Thermal properties of PCM especially during phase transition temperature can strongly affect the performance of a TES system when combined with sensible heat storage material like rocks. The hybrid effect of latent heat and sensible heat storage material in single storage tank is investigated by limited number authors. PCM has thermal buffering characteristic and can be used to stabilize the fluid outlet temperature (Zanganeh et al., 2014). Zanganeh et al. experimentally and numerically studied the effect of encapsulated PCM placed on the top of packed bed of rocks during charging and discharging process (Zanganeh et al., 2015). They concluded that the fluid outlet temperature can be maintained at a higher temperature around the PCM melting point as compared to if only rocks are used. Galione et al. used the numerical model to investigate different combinations of rock filler and encapsulated PCM, forming multi-layered single storage tank. The results show that sensible heat storage material in combination latent heat storage material can lead to a promising TES system (Galione et al., 2015). In our previous work, a comparative thermo-economic analysis of the three different types of thermocline TES systems was presented for medium temperature applications (N. Ahmed et al., 2018). The performance results show that the maximum EDE for pure latent heat TES, sensible heat TES and the combined sensible-latent TES configurations are 95%, 87% and 76% respectively. Morevoer, the cost model predicted that these configurations possess the capacity cost of $42/kWh $37/kWh and $35/kWh, respectively. Based on the developed numerical model and the cost model, a new structured combined sensible-latent heat TES configuration was proposed as the more viable thermocline TES alternative. However, more investigation is needed to explore the effect of different influencing parameters on thermocline characterization for the proposed TES configuration.

It is learnt from the literature study that researchers mostly focused

on either sensible heat storage material or latent heat storage materials for thermocline TES system. Limited work has been reported to combine the advantageous characteristics of both of these types (Gasia et al., 2017). To the best of authors knowledge, till no work has been reported for one tank thermocline TES configuration using the concept of cheap structured sensible heat storage material impregnated with PCM capsules for medium temperature applications. The main objective of this work is to investigate the discharging performance of a new combined sensible-latent TES system. The study takes into account thermocline degradation and the effect of phase change temperature (PCT) on effective discharging time while avoiding the issue of thermal ratcheting.

2. Model formulation

In present work, the geometrical structure of TES consists of solid rod structures positioned vertically in a storage tank with gaps between the rods as shown in Fig. 1. These gaps between SRS are filled by encapsulated spherical shaped PCM capsules of D-Mannitol with a constant porosity. The fluid flow path is of the same length as the tank height. The storage tank is assumed to have distributors to make sure HTF at the inlet is distributed radially uniform. These distributors are not included in the computational domain. The numerical model is formulated for two sensible and latent heat sections of thermal energy storage coupled with the conditions of HTF at their interfaces. Mathematical formulation of energy balance method is done by taking a differential control volume of height Δx along the tank height.

For control volume Δx following assumptions are considered:

(1) The model takes axisymmetric computational domain with incompressible fluid flowing through it.
(2) The distribution of HTF flow and storage filler material is considered uniform in radial direction.
(3) Heat transfer of fluid is governed by advection mode and not by conduction, therefore conduction in fluid along the axial direction is ignored.
(4) Inter particle heat conduction in PCM capsules is negligible.
(5) The tank walls are assumed to be thermally well insulated and losses from storage tank wall to surrounding are negligible.

2.1. Governing equations

By considering above mentioned assumptions energy balance equations are reduced to unsteady axisymmetric problem using Schumann model equations for fluid, SRS and PCM respectively. The numerical model assumes fluid flow as laminar, Newtonian incompressible and its thermos-physical properties are taken as constant over the considered range of temperature. Accordingly, the system of

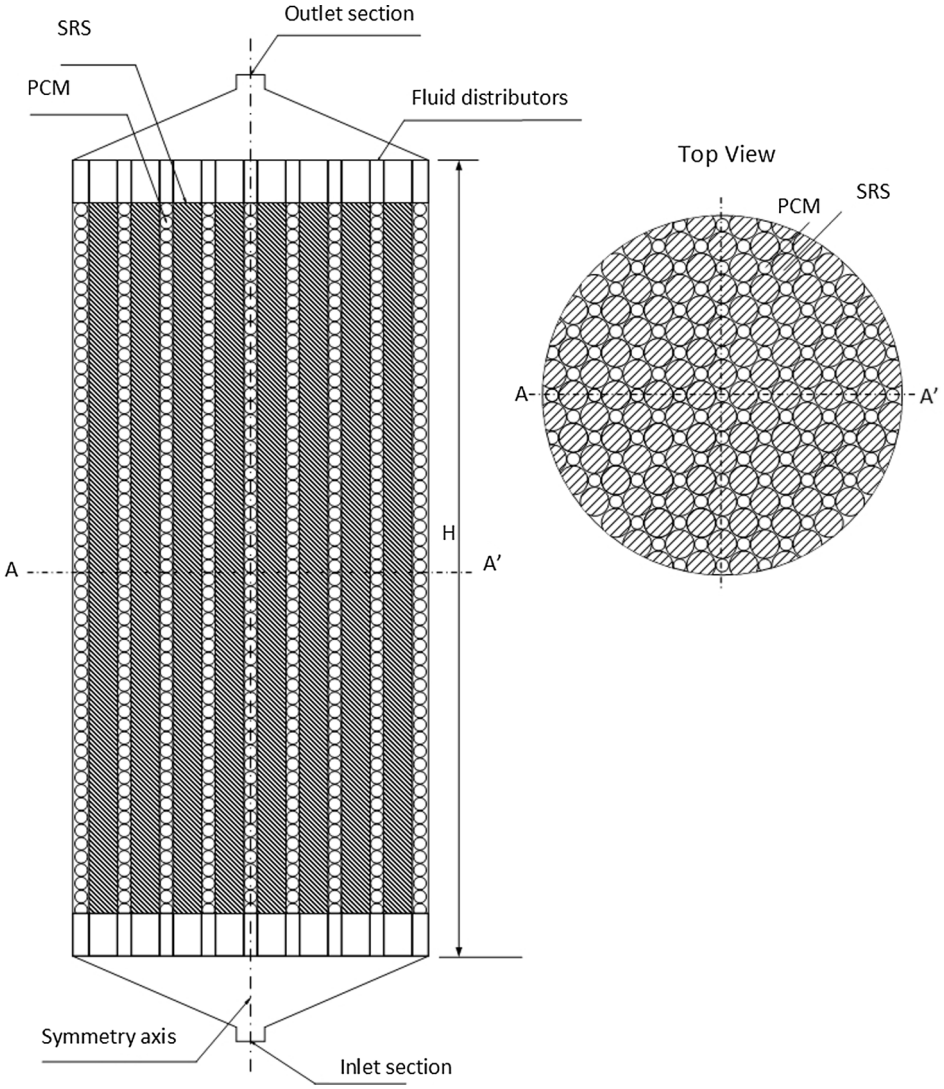

Fig. 1. Schematic of the combined sensible-latent heat storage tank filled with SRS and PCM capsules.

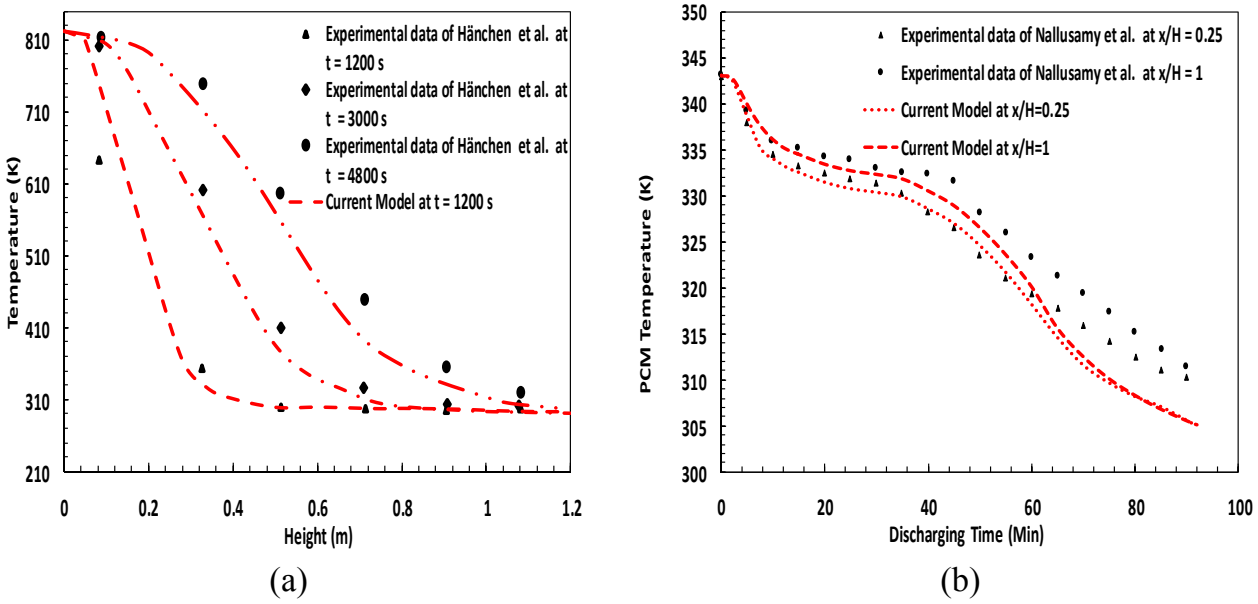

Fig. 2. Comparison between numerical results and experimental data for (a) Sensible heat storage section (b) Latent heat storage section.

Table 1
Geometric parameters and material properties.

Parameter	Value
Height of tank (H), m	7.5
Diameter of tank (D), m	5.0
Density of fluid (ρ_f), kg/m^3	940
Conductivity of fluid (K_f), W/m K	0.10
Specific heat of fluid ($C_{p,f}$), J/kg K	2000
Viscosity of fluid (μ_f), kg/m s	4.90×10^{-04}
Density of SRS (ρ_{SRS}), kg/m^3	3000
Conductivity of SRS (K_{SRS}), W/m K	5.07
Specific heat of SRS ($C_{p,SRS}$), J/kg K	1130
Melting temperature of PCM (T_{mp}), K	438
Latent heat of PCM (L_{PCM}), J/kg	3.0×10^{05}
Specific heat of liquid PCM ($C_{pl,PCM}$), J/kg K	1310
Specific heat of solid PCM ($C_{ps,PCM}$), J/kg K	2360
Density of PCM (ρ_{PCM}), kg/m^3	1490
Conductivity of liquid PCM ($K_{l,PCM}$), W/m K	0.19
Conductivity of solid PCM ($K_{s,PCM}$), W/m K	0.11
Solidus temperature ($T_{solidus}$), K	435.15
Liquidus temperature ($T_{liquidus}$), K	440.8
Inlet temperature of HTF ($T_{f,in}$), K	408
Initial temp of storage tank (T_i), K	468
Threshold temperature (T_h), K	436

governing equations for the proposed thermal energy system can be written as follows,

2.1.1. For fluid

The energy balance equation for fluid entering at a temperature T_{in} in a control volume (AΔx) having interior storage material at an initial temperature T_i and the fluid flowing at a superficial velocity u can be written as(Van Lew et al., 2011).

$$\frac{\partial}{\partial t}(\rho_f \varepsilon T_f) + \nabla.(\rho_f u A_f T_f) = \frac{h_{v,SRS} A_{SRS}}{C_{p,f}}(T_{SRS} - T_f) + S_1 \quad (1)$$

where

$$S_1 = \frac{\partial}{\partial t}\left(\frac{\rho_{PCM} A_{PCM} H_{PCM}(1-\varepsilon)}{C_{p,f}}\right) \quad (2)$$

The unsteady term S_1, is the additional term added to account change in latent heat content of PCM caused by HTF.

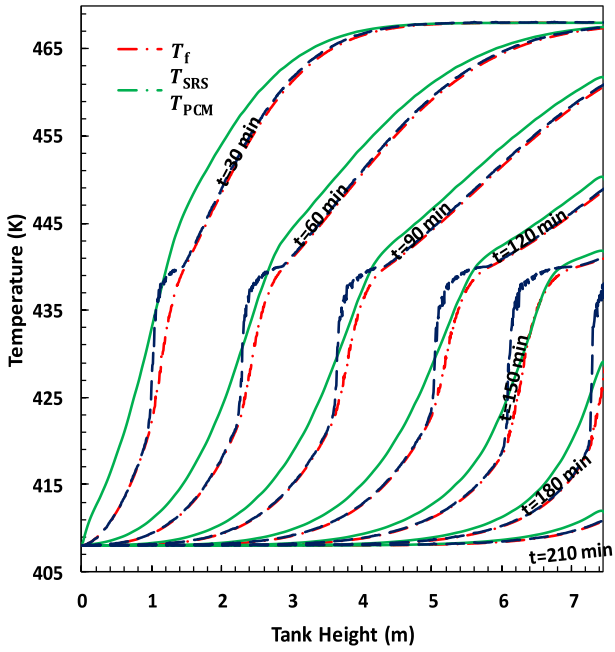

Fig. 3. Temperature distribution of fluid, SRS and PCM along tank axial direction at different discharging moments.

2.1.2. For solid

Similarly, energy balance equation for brick manganese SRS is governed by (Van Lew et al., 2011)

$$\frac{\partial}{\partial t}(\rho_{SRS}(1-\varepsilon)C_{p,SRS}A_f T_{SRS}) = h_{v,SRS}A_{SRS}(T_f - T_{SRS}) \quad (3)$$

Heat transfer exchanged by fluid with the filler storage material is governed by interstitial volumetric heat transfer coefficient h_v, which is a function of overall heat transfer coefficient h_0 of the storage bed. Volumetric heat transfer coefficient for both PCM and SRS are formulated separately using the following correlations (Kim, 1993)

$$h_v = \frac{6h_0(1-\varepsilon)}{D} \quad (4)$$

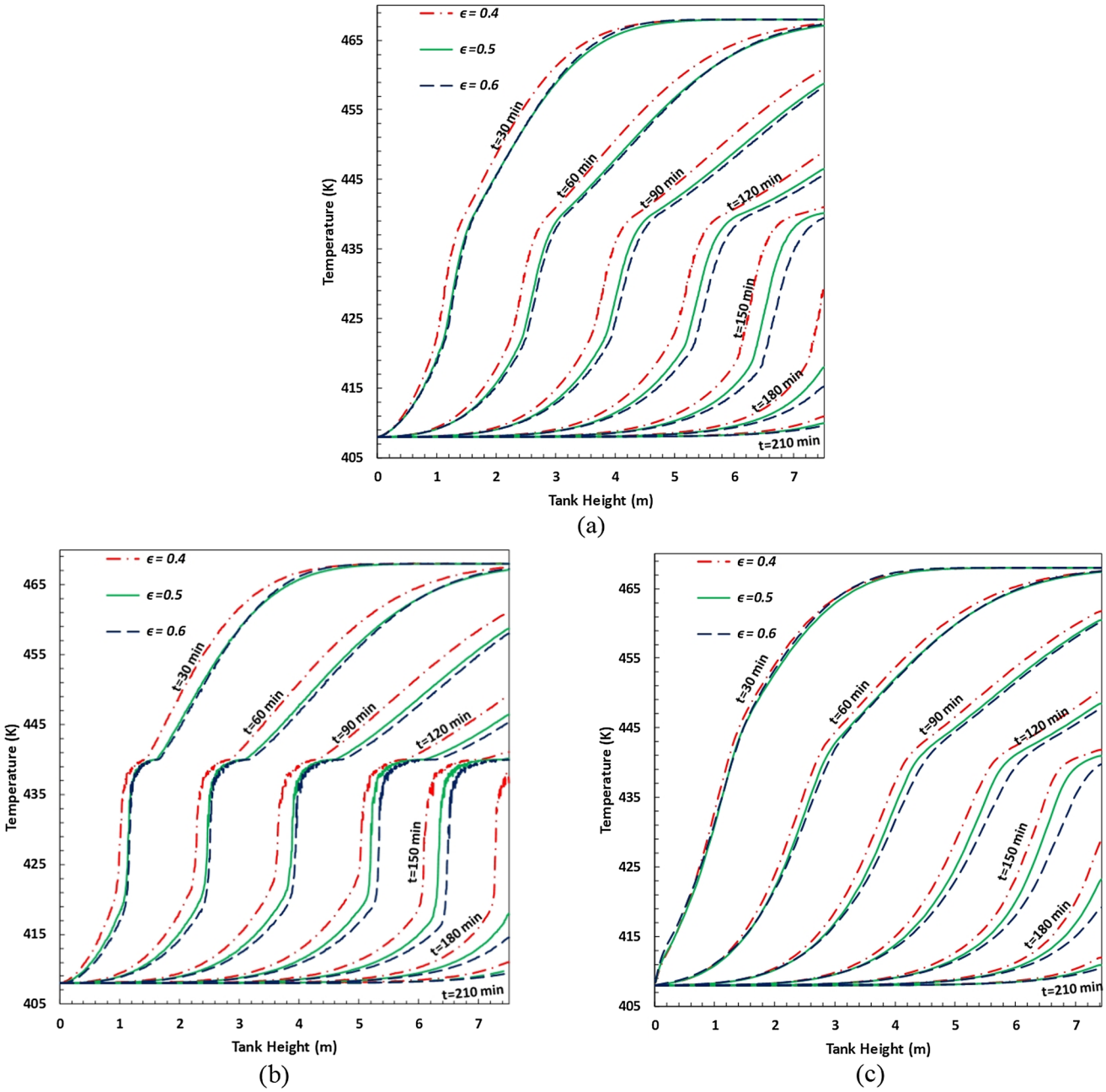

Fig. 4. Temperature distribution along axial direction at different discharging moments for different porosities (a) fluid (b) PCM capsules (c) SRS.

External thermal resistance caused by the fluid due to convection on the external surface of PCM and SRS is a function of storage bed porosity, thermos-physical properties of HTF and its Reynolds number. And the Nusselt number is calculated using the following relation suggested by Wakao et al. (Wakao et al., 1979)

$$Nu = 2 + 1.1(6(1-\varepsilon)^{0.6})\mathrm{Re}^{0.6}\,\mathrm{Pr}^{1/3} \tag{5}$$

where Reynolds number and Prandtl number are formulated using the correlations

$$\mathrm{Re} = \frac{\rho u D}{\mu};\ Pr = \frac{\mu C_p}{K} \tag{6}$$

2.1.3. For PCM material

Phase change phenomenon in encapsulated PCM during the discharge process is formulated using enthalpy method (Felix Regin et al., 2009). The enthalpy equation for phase change storage bed material is governed by

$$\frac{\partial}{\partial t}(\rho_{\mathrm{PCM}}(1-\varepsilon)H_{\mathrm{PCM}}) = h_{\mathrm{v,PCM}}(T_f - T_{\mathrm{PCM}}) \tag{7}$$

where the value of H_{PCM} depends on the region in which it lies during solidification or melting and is a function of T_{PCM}. The temperature range of phase change process of PCM is divided into the following three sub-states.

i. When in solid phase

$$H_{\mathrm{PCM}} = C_{\mathrm{ps,PCM}}\,T_{\mathrm{PCM}}\ \ T_{\mathrm{PCM}} \leqslant T_{\mathrm{solidus}} \tag{8}$$

ii. When in solid–liquid phase

The enthalpy change occurs over a range of temperature when PCM

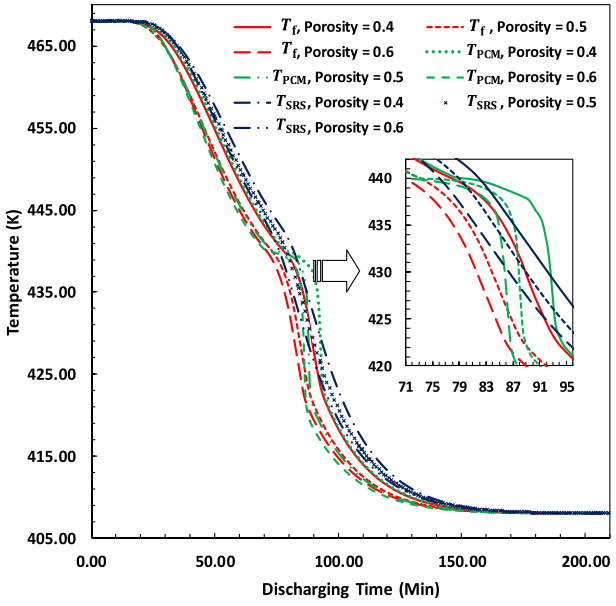

Fig. 5. Temperature profiles of fluid, PCM and SRS at x = H/2 as a function of discharging time for different porosities.

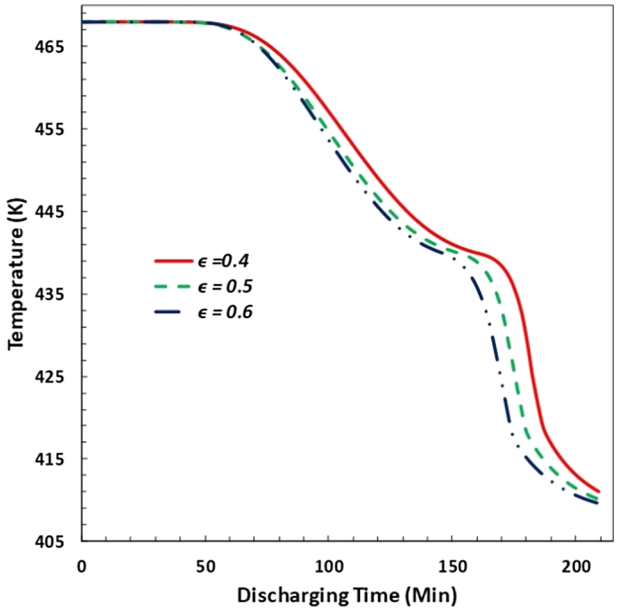

Fig. 7. Temperature profile of fluid at outlet with discharging time for different porosities.

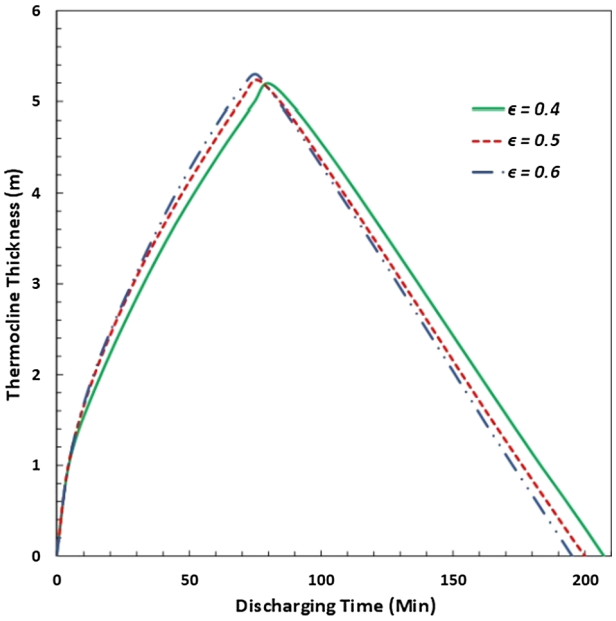

Fig. 6. Thermocline thickness formation as function of discharging time for different porosities.

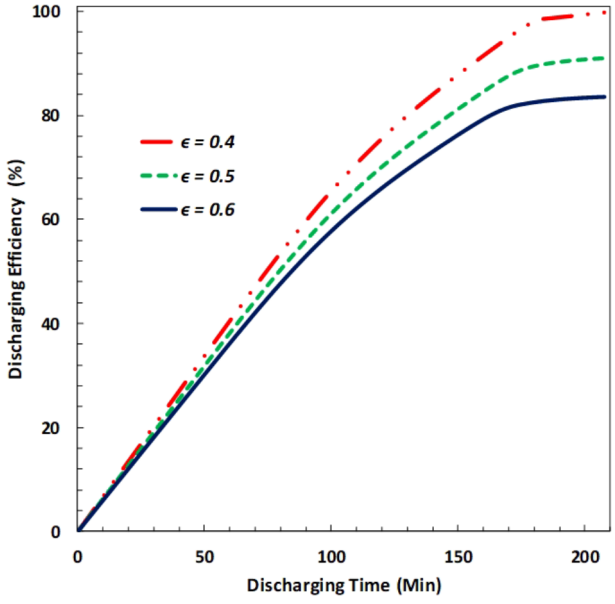

Fig. 8. Discharging efficiency of HTES as a function of time for different porosities.

just starts changing phase with latent heat of melting supplied over this temperature range and it is neither fully in solid state nor fully liquid state.

$$H_{PCM} = C_{ps,PCM}T_{PCM} + \frac{L_{PCM}}{(T_{liquidus} - T_{solidus})}(T_{PCM} - T_{solidus})\ T_{liquidus} < T_{PCM} < T_{solidus} \quad (9)$$

iii. When PCM is fully in liquid phase

$$H_{PCM} = C_{ps,PCM}(T_{mp} - T_i) + C_{pl,PCM}(T_{final} - T_{mp}) + L_{PCM}\ T_{PCM} \geqslant T_{liquidus} \quad (10)$$

This enthalpy equation for PCM packed bed is used to calculate PCM temperature with enthalpy being dependent variable and temperature as an independent variable. The calculated enthalpy value as a function of storage tank axial location and time is used to study thermal stratification and thermocline layer degradation after each discharging cycle.

An important parameter used to evaluate the discharging performance of combined sensible-latent heat TES is thermocline thickness, W_{tc} and is defined as the covering length of thermocline region (Xu et al., 2012).

$$W_{tc} = \begin{cases} H(T_h) - H(T_c) & (T_{f,inlet} \leqslant T_c)\&(T_{f,out} \geqslant T_h) \\ H(T_h) - 0 & (T_{f,inlet} > T_c) \\ H - H(T_c) & (T_{f,out} < T_h) \end{cases} \quad (11)$$

In the current study for the evaluation of thermocline thickness T_c, the critical cold temperature and T_h, the critical hot temperature are taken as 412 K and 468 K, respectively.

The usefulness of energy recovered from TES during discharging cycles is quantified using discharging efficiency. Discharging efficiency

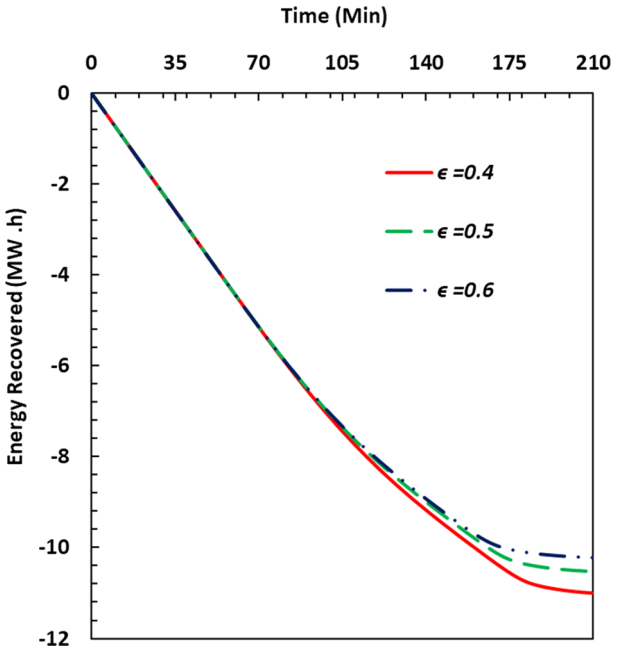

Fig. 9. Total energy recovered during discharging process for different porosities.

Table 2
Fractions of thermal energy exhibited by the TES system at the end of t = 150 min relative to the total energy recovered.

Parameter		$f_{PCM,}$ (%)	$f_{SRS,}$ (%)	$f_{HTF,}$ (%)
Porosity	0.4	45.82	45.62	8.55
	0.5	49.4	39.43	11.16
	0.6	53.8	32.4	13.74
SRS size	0.06	47.5	40.4	12.1
	0.08	49.4	39.43	11.16
	0.1	51.2	38.54	10.26
Velocity	0.001	52.1	37.2	10.7
	0.002	49.4	39.43	11.16
	0.003	48.4	40.17	11.4

is defined as the ratio of the amount of useful energy extracted from storage tank during the whole discharging process to the maximum energy stored initially before the start of discharge process. It is given as

$$\eta_{dis} = \frac{\int_0^{t_c} \dot{m} C_p (T_{f,out} - T_{f,inlet}) dt}{Q_{initially}} \quad (12)$$

$$Q_{initially} = Q_f + Q_{PCM} + Q_{SRS} \quad (13)$$

where

$$Q_f = (\rho_f V_f C_{p,f})(T_{final} - T_{initial}) \quad (14)$$

$$Q_{PCM} = (X\rho_l V_{PCM} L_{PCM}) + (\rho_s V_{PCM} C_{p,s}(T_{mp} - T_{initial})) + (\rho_l V_{PCM} C_{p,l}(T_{PCM} - T_{mp})) \quad (15)$$

$$Q_{SRS} = (\rho_{SRS} V_{SRS} C_{p,SRS})(T_{final} - T_{initial}) \quad (16)$$

where t_c is the cut off time during discharging process at which HTF outlet temperature drops below the threshold value. Threshold value depends on specific process to which TES is integrated and in present work it is taken as 436 K which is just below the melting point of PCM and is chosen to take advantage of outlet temperature stabilization characteristic of PCM (Zanganeh et al., 2014). It means that the only energy extracted above ($T_{initial}$ − 32) is considered to be useful for application specific process. Practical storage capability of TES closely depends on threshold temperature of a particular application (Merlin et al., 2016).

The fractions of thermal energy retained by SRS f_{SRS} and latent heat storage material f_{PCM}, relative to the total energy stored in TES tank are formulated using the relations (Zanganeh et al., 2014)

$$f_{SRS} = \frac{E_{SRS}}{E_{PCM} + E_{HTF} + E_{SRS}} \quad (17)$$

$$f_{PCM} = \frac{E_{PCM}}{E_{SRS} + E_{HTF} + E_{PCM}} \quad (18)$$

where E_{SRS}, E_{HTF} and E_{PCM} is the amount of thermal energy exhibited by SRS, fluid and PCM storage material, respectively.

2.2. Initial and boundary conditions

The formulated equations for the numerical model are solved using the following suitable set of initial and boundary conditions.

(i) Initial condition: At t= 0 $T_i = T_f = T_{SRS} = T_{PCM} = 468$ K (19)

(ii) B.C. at inlet: At t> 0 $T_f = 408$ K, $u = 0.002$ m/s (20)

(iii) B.C. at symmetry axis: $\frac{dT_f}{dy} = 0, \quad \frac{du}{dy} = \frac{dv}{dy} = 0$ (21)

(iv) B.C. at outer wall of tank: $\frac{dT_f}{dy} = 0, \quad \frac{dT_{PCM}}{dy} = 0, \quad \frac{dT_{SRS}}{dy} = 0, \quad u = v = 0$ (22)

(v) B. C. at outlet of tank: $\frac{dT_f}{dx} = 0, \quad \frac{dT_{PCM}}{dx} = 0, \quad \frac{dT_{SRS}}{dx} = 0, \quad P = 0$ (23)

2.3. Numerical modeling

The transient numerical model is based on two-phase Schumann model equations formulated separately for fluid, sensible and latent heat storage materials. During discharging process, the cold HTF at a temperature T_{in} flows from the bottom of storage tank. It gains heat energy from the storage filler (PCM and SRS) causing internal stored energy of TES to be decreased as the time passes. After several hours of discharging cycles HTF and the filler material have almost the same low temperature, the TES tank is said to be in completely discharged state. The geometric configuration of computational domain consists of a 2D axisymmetric cylindrical storage tank having a height of 7.5 m and a diameter of 5 m. The mesh grid is quadrilateral dominant having cells with a discretization size around 7 mm. The numerical model is implemented by using formulated energy balance equations as User Defined Scalar (UDS) transport equations in FLUENT using SIMPLE scheme. The gravity direction is in-line with axial flow. First order implicit scheme is used for the transient formulation of temporal terms. Spatial discretization is performed using Least Square Cell based method with first order upwind schemes. The solution for numerical model is assumed to be converged when residuals for the UDS and flow variables approach values less than 10^{-6} and 10^{-3} respectively.

2.4. Model validation

The developed numerical model is validated separately for both sensible heat storage material and latent heat storage material. The model for sensible heat storage section is authenticated using the experimental data of pilot scale thermal storage prototype ARIANE containing a packed bed of rocks as storage material and is shown in Fig. 2(a) (Hänchen et al., 2011). The formulated numerical model is

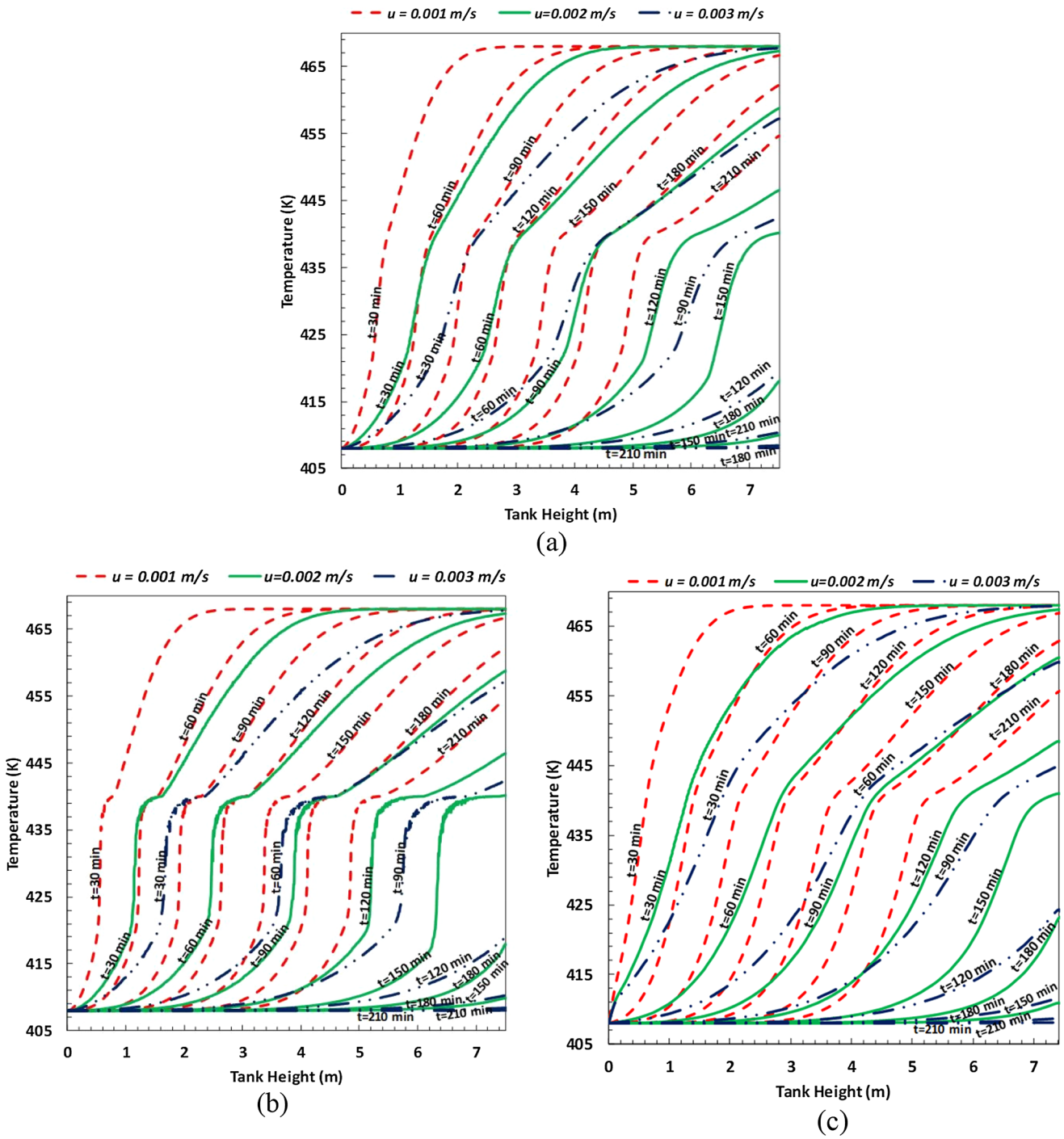

Fig. 10. Temperature distribution along axial direction at different discharging moments for different fluid inlet velocities (a) Fluid (b) PCM capsules (c) SRS.

simulated using dimensions and properties taken from previous work by the same group (Hänchen et al., 2011; Meier et al., 1991). The implementation of developed numerical model for the latent heat storage section is tested by comparing simulated results with the experimental results stated by Nallusamy et al. (Nallusamy et al., 2007) and is shown in Fig. 2(b). The numerically predicted results show a reasonable trend as reported in experimental measurements (Nallusamy et al., 2007). However, a little discrepancy may be attributed to following reasons that capsule film thickness conductivity is ignored in current studies but included in the experimental results. Also there is uncertainty about the exact placement of thermocouples. An error analysis between the experimental data and simulated results indicate a maximum error of 8.6% and 3% for sensible and latent heat sections, respectively. Agreement of the numerically predicted results with the experimental results (Hänchen et al., 2011; Nallusamy et al., 2007) confirms the validity of the formulated model. Thus forming the foundation for parametric analysis which is presented and discussed in the next section.

3. Results and discussion

Thermal performance of a single TES tank is associated with the thickness of thermocline region. The lower the thickness, the higher is effective discharging efficiency (Xu et al., 2012). However, thermocline formation is characterized by different operating factors. The results presented in current section use ENE LQ-D400 as a HTF with geometric

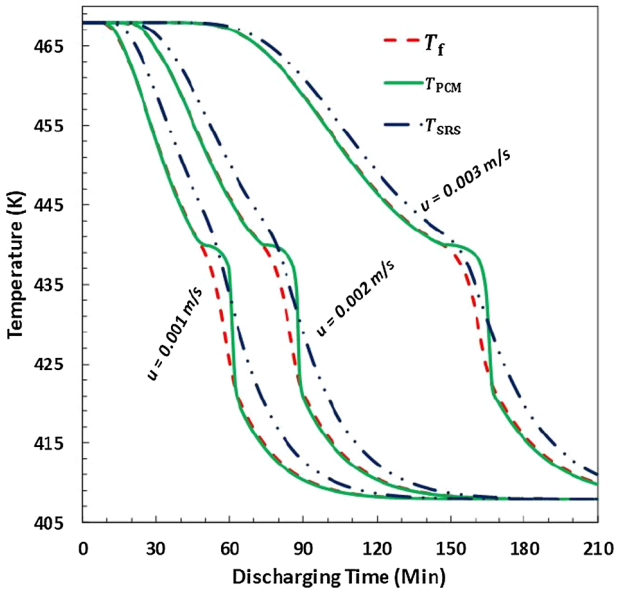

Fig. 11. Temperature profiles of fluid, PCM and SRS at x = H/2 as a function of discharging time for different inlet velocities.

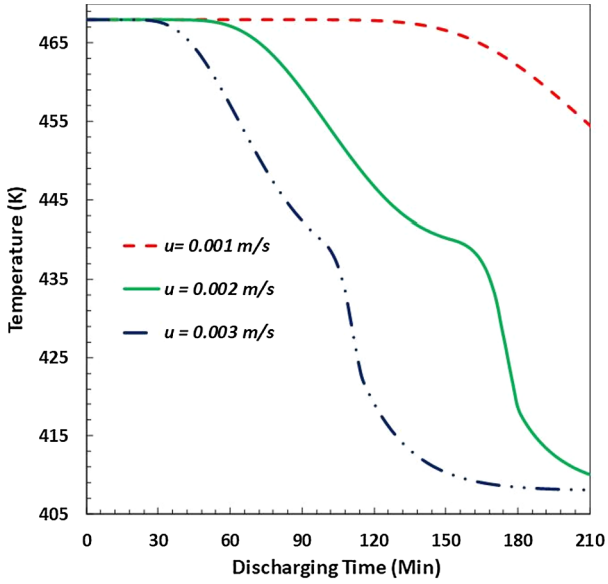

Fig. 13. Temperature profile of fluid at outlet with discharging time for different inlet velocities.

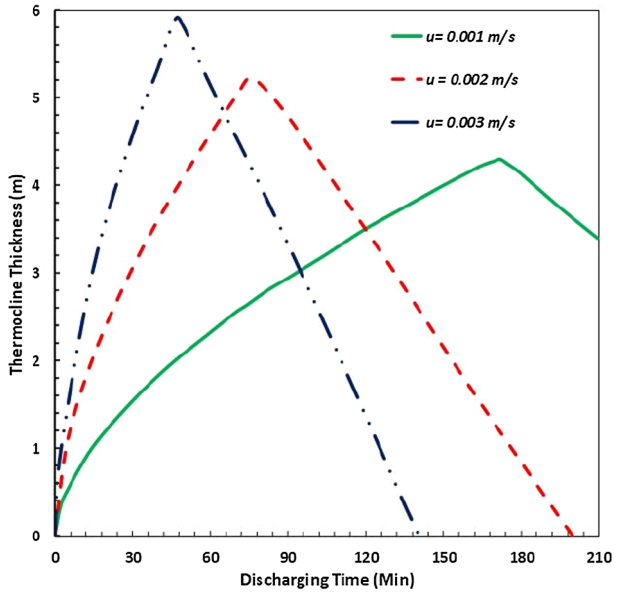

Fig. 12. Thermocline thickness formation as function of discharging time for different fluid inlet velocities.

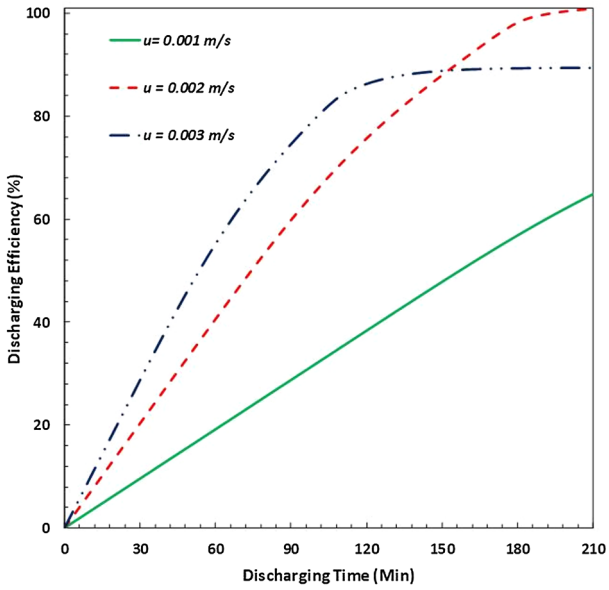

Fig. 14. Discharging efficiency of HTES as a function of time for different inlet velocities.

parameters and material properties presented in Table1. Fig. 3 shows the temperature distribution of HTF, PCM and SRS along the axial direction of the storage tank at different discharging moments. The numerical simulations consider $u = 0.002$ m/s, $\varepsilon = 0.4$ having PCM and SRS constant diameter of 0.08 m and 0.02 m, respectively. Over the discharging period thermocline layer is shifted upward, leaving more cold region at the bottom section and resulting in reduced hot areas at the top section of the tank. Moreover, it can be observed from the reduced slopes of temperature profiles that the thermocline layer thickness keeps on expanding as the discharging time increases. As can be seen from the figure, the temperature history of PCM dictates that temperature reduction of HTF is high until PCM arrives at its phase change temperature i.e. 438 K. At this point it increases the slope of fluid temperature profile. This is because hot water in the storage tank losses its sensible heat to cold inlet HTF due to mixing at a temperature close to the phase transition of PCM. After that moment the reduction in PCM temperature is very small or negligible over a discharging period as long as PCM keeps on releasing its latent heat. Meanwhile the liquid fraction in PCM starts to decrease.

Moreover, the results in Fig. 3 also show that after every discharging time there are tiny waviness of temperature profile in PCM capsules along the tank height during the phase transition temperature range. As the same was revealed by Tan et al. (Tan et al., 2009), is due to the presence of unstable fluid flow structure at the bottom of capsule. It is also caused by the presence of variable temperature zones possessing different thermal conductivity in the mushy zone of PCM. SRS structure of brick manganese release its heat energy slowly as compared to the latent heat storage material. Though after initial discharging of 30 minutes (min) it is at a higher temperature than the PCM except during phase transition period. However, it is interesting to note that as discharging time passes the temperature difference between HTF and SRS becomes lower, while PCM trying to keep HTF temperature closer

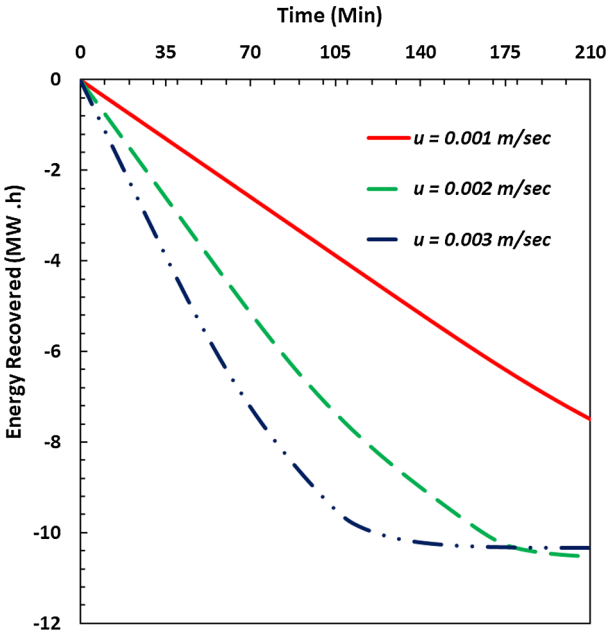

Fig. 15. Total energy recovered during discharging process for fluid inlet velocities.

to its melting point during phase transition. For instance, after a discharging time of 30 min along the tank height at H = 1.4 m, the maximum temperature difference between SRS and fluid during PCT range is 6.4 K. As the discharging process proceeds, this temperature difference reduces until it becomes zero at H = 6.6 m after t = 150 min.

Hence, the temperature profiles of combined sensible-latent heat storage unit show that there is a thermal buffering effect for thermocline region formation along tank height where PCM capsules are at its phase transition stage. HTF passing through this region is forced to remain close to PCM's melting point affecting the thermal gradient of fluid. This allows comparatively longer discharging time and greater thermal energy filling of the whole storage tank. Therefore, the thermal stabilization characteristic of PCM can be utilized to enhance effective discharging time (EDT) of TES. But it important that the PCT is chosen carefully depending upon the fluid outlet temperature to be used for a specific medium temperature application.

3.1. Effect of porosity

In order to investigate the effect of different porosities on discharging performance of combined sensible-latent heat TES system, three different porosities of 0.4, 0.5 and 0.6 are simulated for a fixed $u = 0.002$ m/s, $D_{SRS} = 0.08$ m, $D_{PCM} = 0.02$ m. It can be seen clearly from Fig. 4, the TES systems having lower porosity values show better performance and improved temperature profiles at different discharging moments. The temperature profiles for fluid, SRS and PCM are observed to be at a higher value for $\varepsilon = 0.4$ than $\varepsilon = 0.5$ and the least is for $\varepsilon = 0.6$. This is because lower porosity means smaller path is available for fluid flow and more contact area with PCM and SRS storage material causing increased heat transfer. These different behaviors of temperature profiles at different porosities directly lead to different thermal performances of TES system.

For the convenience of porosity effect analysis, the temperature profile of fluid and storage material at x = H/2 as a function of discharging time is chosen as the representative profile. The results in Fig. 5 illustrate that the temperature profile remains almost at an initial temperature of 468 K for $\varepsilon = 0.4$ until 25 min, after that it starts to discharge more quickly except during the PCT range. It becomes fully discharged after 150 min when the fluid at inlet and tank has the same temperature i.e. 408 K. Whereas for $\varepsilon = 0.5$ and $\varepsilon = 0.6$, the TES units are in fully discharged state after 140 min and 136 min, respectively.

The Thermocline thickness profile is a key indicator to predict the thermal performance of single tank energy storage and can clearly explain the formation of thermal gradients for fluid, SRS and PCM capsules along the flow direction. Fig. 6 shows that initially there is a sharp increase in thermocline thickness and when the cold inlet fluid starts gaining heat energy, the growth in thermocline becomes slower. It attains maximum value when the thermocline region reaches at outlet and after that there is a linear decrease in thermocline thickness. The results show that thermocline thickness increases with the increase of porosity. The maximum thermocline thickness achieved is for $\varepsilon = 0.6$ of 5.33 m at a discharging period of 75 min and the least is for $\varepsilon = 0.4$ of 5.19 m at t = 80 min.

The lower thermocline thickness effect at lower porosities helps to maintain the fluid at the outlet at a higher temperature than the TES tanks with higher porosities. It is evident from Fig. 7, showing the effect of porosity on the outlet temperature of the fluid. The fluid remains at a hot temperature of 468 K for several minutes, then it decreases almost linearly until it reaches phase transition temperature of PCM. During this period, it tries to maintain the fluid outlet temperature around its PCT prolonging EDT. It should be noted that when fluid outlet temperature drops below the threshold value of 436 K, the output energy cannot be further utilized to perform useful work by the assumed specific application. The outlet threshold temperature is chosen close to the melting point of PCM filler because PCM capsules placed nearby outlet of TES try to stabilize the temperature of outgoing fluid around its phase transition temperature. The results indicate that as the porosity increases fluid outlet temperature drops more quickly. The results in Fig. 8 show that initially discharging efficiency increases linearly for all three porosities and after several minutes the increment becomes slow. This is because the thermocline region reaches at the outlet and when stored energy is completely discharged, the efficiency becomes 100%. Furthermore, the results indicate that EDE of thermocline TES decreases as porosity increases. The maximum EDE achieved for $\varepsilon = 0.4$ is 96.5% followed by $\varepsilon = 0.5$ with 86.7% and the least at $\varepsilon = 0.6$ with 79.2%.

The results in Fig. 9 indicate that the discharging performance is clearly affected by the amount of energy extracted from fully charged TES system during recovery cycles as a function of porosity. The energy utilization of combined sensible latent heat TES increases as porosity decreases. This caused by increased heat transfer rates and the availability of heat driving force, arising due to higher temperature difference between fluid and the storage media. After a discharging period of 210 min, the amount of energy recovered is10.2 MWh, 10.6 MWh and 11.1 MWh for a porosity value of 0.6, 0.5 and 0.4 respectively. This can also be explained by analyzing the fractions of energy exhibited by the HTF and storage material (SRS, PCM) relative to the total energy recovered for different porosity values. Table 2 shows that as porosity of the filler material is increased, the fractions of thermal energy stored by phase change material and HTF increases while for SRS it decreases. After a discharging period of 150 min PCM and SRS retain 45.8% and 45.6% of total thermal energy for $\varepsilon = 0.4$. Whereas with a porosity value of 0.6, the energy fraction is increased to 53.8% and decreased to 32.4% for PCM and SRS respectively.

3.2. Effect of fluid inlet velocity

In this section effect of fluid inlet velocity is investigated on the performance of thermocline combined sensible-latent heat TES tank. Fig. 10 shows the temperature distribution of fluid, PCM and SRS storage material along tank height for different inlet velocities of 0.001, 0.002 and 0.003 m/s, respectively at various discharging moments. The numerical simulations are carried out for a fixed $\varepsilon = 0.5$, $D_{SRS} = 0.08$ m and $D_{PCM} = 0.02$ m. The results show that with the decrease in fluid inlet velocity longer discharging time is observed, causing reduced thermocline thickness. For instance, at a velocity of 0.003 m/s the

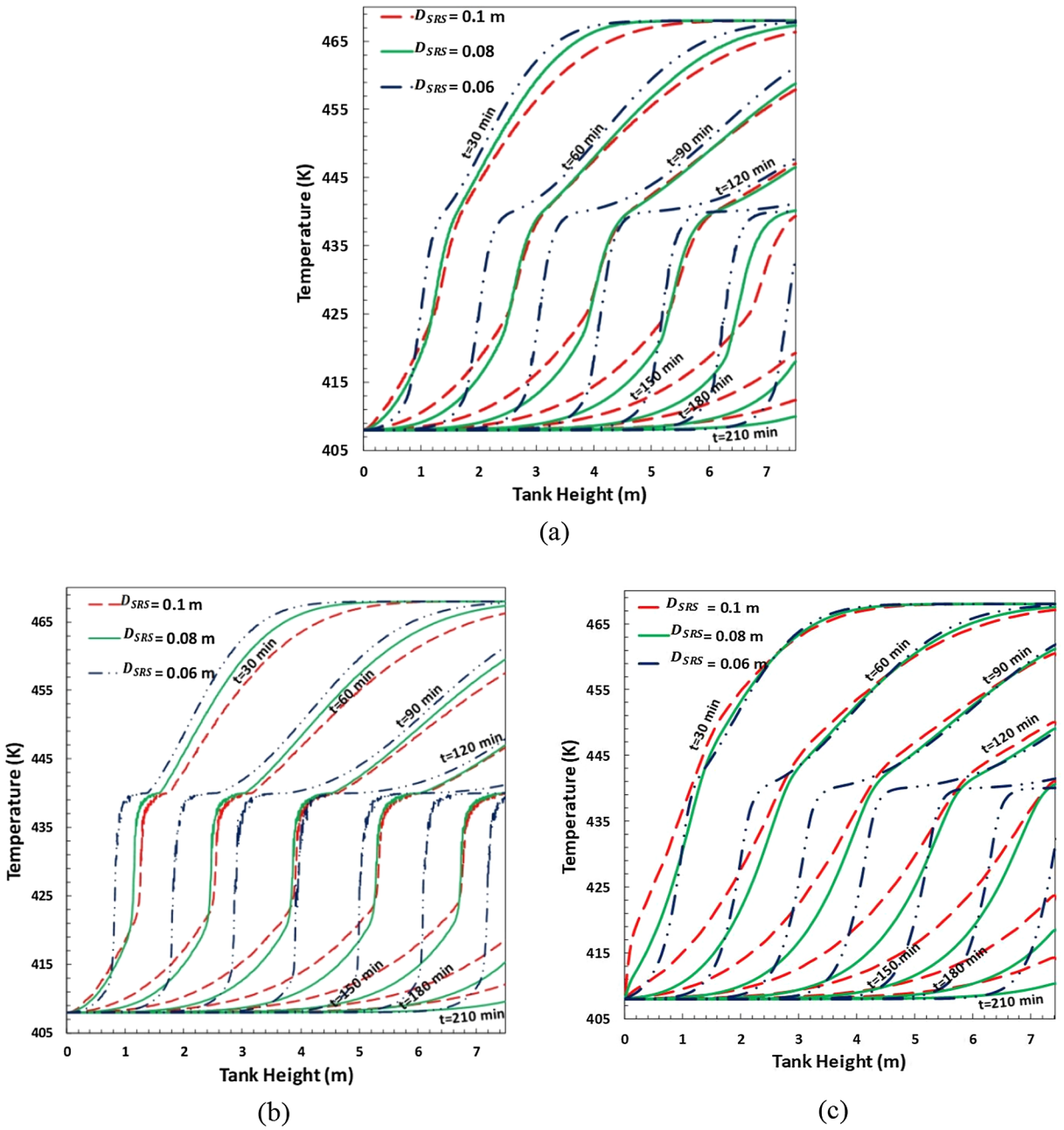

Fig. 16. Temperature distribution along axial direction at different discharging moments for different SRS feature sizes (a) fluid (b) PCM capsules (c) SRS.

temperature distribution of fluid, PCM and SRS have thermal gradient covering almost entire tank height only after 30 min of discharging. This is associated with the fact that higher inlet fluid velocity causes quick solidification of the downstream PCM capsules due to higher heat transfer rate between HTF and the storage material. The temperature profiles of fluid, PCM and SRS at × = H/2 in Fig. 11 show that the lower the fluid velocity, the longer the time taken by the PCM to reach below its phase transition temperature. For u = 0.003 m/s PCM arrives at its melting point only after 59 min, while at the velocities of 0.002 m/s and 0.003 m/s it takes approximately 85 min and 162 min respectively. The effect of fluid inlet velocity on the formation and degradation of thermocline thickness is shown in Fig. 12. As can be seen that the maximum thermocline thicknesses achieved for the velocities of 0.001, 0.002, 0.003 m/s are 4.3 m, 5.2 m, 5.9 m after the discharging times of 172 min, 75 min and 47 min, respectively.

Fig. 13 shows that HTF outlet temperature takes shorter time to fall below the threshold temperature for larger inlet fluid velocities, predicting reduced EDE. EDT is calculated to be 307 min, 166 min and 105 min as the velocity is varied to be 0.001, 0.002 and 0.003 m/s respectively. Due to this reason, as shown in Fig. 14, the discharging efficiency of the TES system for u = 0.003 m/s first increase linearly higher as compared to the efficiency at lower velocities. But then it becomes almost constant after a period of 147 min where the temperature difference between HTF and the storage material happens to be very small. Moreover, the results in Fig. 15 illustrate that it takes more time for lower velocities to recover the initially stored energy. The graph shows that the amount of energy extracted at the end of t = 150 min is 89%, 81% and 49% for 0.003, 0.002 and 0.001 m/sec, respectively. Moreover, as the velocity of fluid increases, the fractions of energy retained by PCM is reduced while for SRS it increases This is because at higher velocities, the fluid heat exchange with PCM capsules is enhanced relative to that with SRS and is depicted in Table 2.

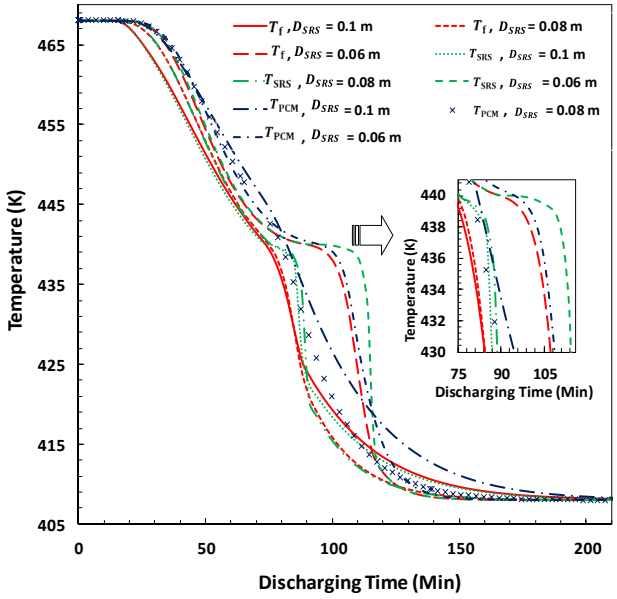

Fig. 17. Temperature profiles at x = H/2 of fluid, PCM and SRS as a function of discharging time for different SRS feature sizes.

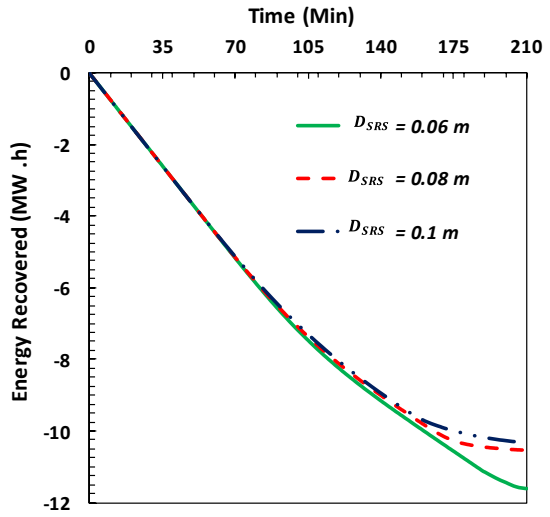

Fig. 18. Total energy recovered during discharging process for different SRS feature sizes.

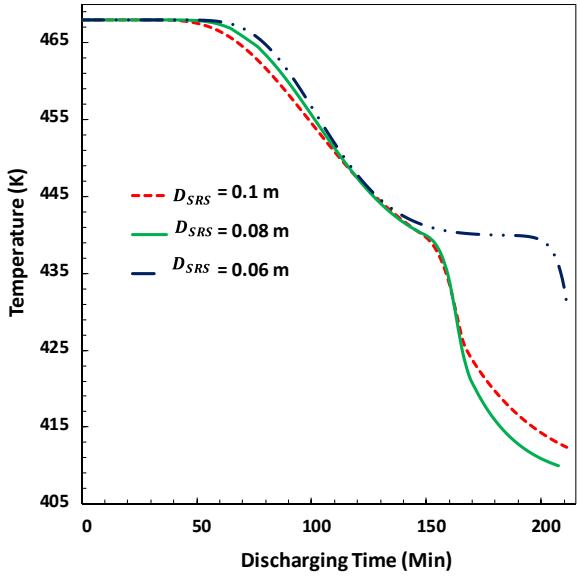

Fig. 19. Temperature profile of fluid at outlet with discharging time for different SRS feature sizes.

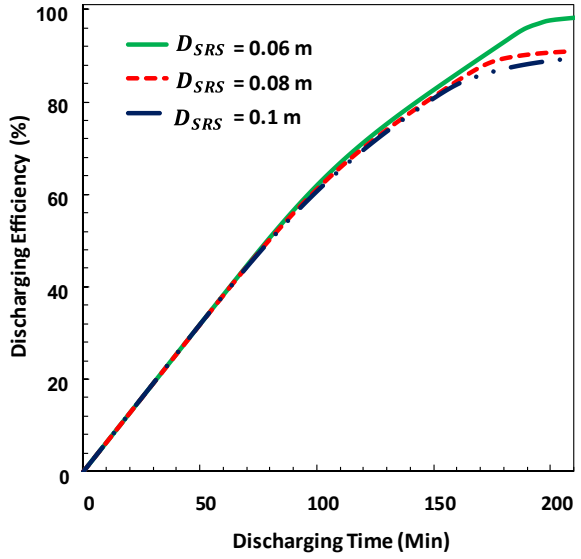

Fig. 20. Discharging efficiency of HTES as a function of time for different SRS feature sizes.

3.3. Effect of SRS feature size

The effect of SRS feature size (impregnated with PCM capsules of uniform size) on the thermocline performance of hybrid TES system is investigated by using different diameters of 0.06, 0.08 and 0.1 m while keeping constant $\varepsilon = 0.5$, $u = 0.002$ m/s, $D_{PCM} = 0.02$ m. The temperature profiles of HTF and combined storage material along the axial direction are shown in Fig. 16. The results show that for $D_{SRS} = 0.06$ m TES system has the best discharging performance as indicated by the shortest thermocline region, followed by $D_{SRS} = 0.08$ m and $D_{SRS} = 0.1$ m exhibits the least. This is because with the increase of SRS feature size, the thermocline region is enlarged due to the reduced heat transfer rate between solid rods and HTF. It can be seen in Fig. 17 that after a discharging period of 30 min at x = H/2, the fluid temperature difference between $D_{SRS} = 0.08$ m and $D_{SRS} = 0.06$ m is 1.95 K. After t = 90 min this difference increases to 17.85 K, exhibiting that the TES unit with smaller feature sizes improve the discharging performance. Fig. 18 shows the total energy recovered during discharging process as a function of time for different SRS feature sizes. The results exhibit that greater amount of energy is recovered for $D_{SRS} = 0.06$ m due to enhanced heat transfer coefficient between smaller sized SRS and HTF. The same effect is illustrated by the energy fraction values for different diameters of SRS in Table 2.

The effect of SRS feature size on the temperature profile of fluid at the outlet is shown in Fig. 19. The use of smaller SRS feature size combined with PCM shows stabilization of outlet temperature for a longer period resulting in enhanced EDT. As can be seen for $D_{SRS} = 0.1$ m and $D_{SRS} = 0.08$ m the EDT is 157 min and 166 min respectively. Whereas, for $D_{SRS} = 0.06$ m the effective discharging time is enhanced to 207 min. Moreover, as shown in Fig. 20, this results in higher EDE of 98% for $D_{SRS} = 0.06$ m followed by 86.7% and 82.9% for $D_{SRS} = 0.08$ m and $D_{SRS} = 0.1$ m, respectively. Therefore, the new combined sensible-latent heat TES configuration containing smaller diameter sized SRS impregnated with PCM capsules is preferred here for higher EDE and reduced thermocline thickness.

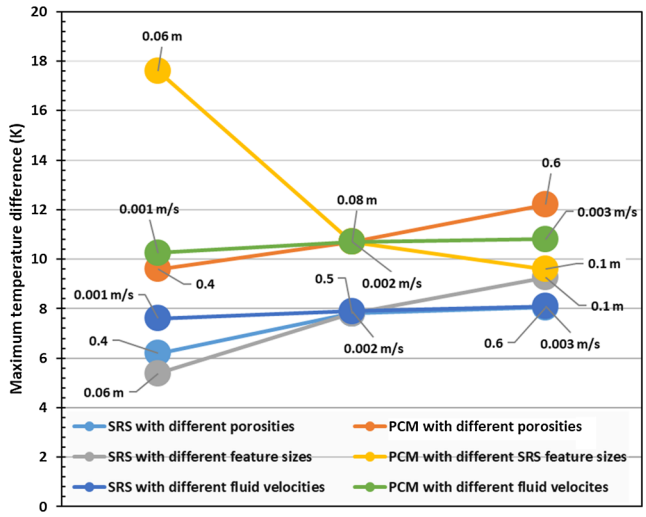

Fig. 21. Variations in the maximum temperature differences between HTF and storage filler (PCM and SRS) as a function of different performance influencing parameters.

Table 3
EDT, EDE and maximum thermocline thickness achieved as a function of different influencing parameters.

Parameter		EDT (min)	EDE (%)	Max- thermocline thickness (m)
Porosity	0.4	174.43	96.5	5.19
	0.5	166.53	86.7	5.22
	0.6	159.75	79.2	5.33
SRS feature Size (m)	0.06	207	98.2	4.81
	0.08	166.53	86.7	5.22
	0.1	156.98	82.9	5.84
Velocity (m/s)	0.001	307	96.1	4.30
	0.002	166.53	86.7	5.22
	0.003	104.70	81.9	5.90

In order to achieve improved heat transfer rate between the HTF and the storage material with reduced thermocline thickness, the heat transfer coefficient should be large enough to give small temperature difference between HTF and the storage media. Fig. 21. shows variations in the maximum temperature differences between HTF and the storage material (PCM and SRS) as a function of different values of porosity, SRS feature size and fluid inlet velocity. The results show that as the porosity of storage material increases, the maximum temperature difference (T_{SRS} - T_{HTF}) and (T_{PCM} - T_{HTF}) is enlarged. This indicates less effective heat transfer which results into reduced thermal energy recovery and higher thermocline thicknesses. When the SRS feature size is increased from 0.06 m to 0.1 m, the maximum temperature difference (T_{SRS} - T_{HTF}) increases from 5.39 K to 9.26 K, respectively. This is because of lower heat transfer extraction by HTF from large size SRS. Whereas, on the contrary maximum temperature difference (T_{PCM} - T_{HTF}) for PCM decreases causing enhanced heat transfer rate with small size PCM capsules. Moreover, the maximum temperature difference increases for both SRS and PCM capsules for higher fluid inlet velocities. With the increase in velocity from 0.001 to 0.003 m/s, the maximum temperature difference for SRS increases from 7.6 K to 8.1 K respectively. Whereas, for PCM it increases from 10.25 to 10.8 K. This is because at lower velocities more time is spent by the HTF to exchange heat with the storage material in comparison to higher velocities. Therefore, the overall results as illustrated in Table 3, show that the influence of porosity, SRS feature size and fluid velocities on heat transfer rate play a crucial role in determining thermocline behavior of combined sensible-latent heat TES system.

4. Conclusions

In current the study, transient two-phase Schumann model equations are evaluated numerically to investigate the influence of combined sensible-latent heat storage material on thermocline characterization of the new proposed TES configuration. A detailed parametric sensitivity analysis is presented by examining various numerical results, including temperature distribution of HTF, PCM and SRS, thermocline thickness as a function of time, formation of thermocline profiles, fractions of energy recovered, effective discharging time and discharging efficiency. Moreover, the model is used to study heat transfer between fluid and the combined sensible-latent heat storage material, as well as the effect of PCM phase transition on thermocline degradation is presented. This study contributes to better understanding of discharging behavior of the combined sensible-latent heat TES system working on the principle of thermocline. Thus providing a hint to optimize the design and operational parameters within practical constraints.

Main findings from the current study are summarized below.

(1) The thermocline layer moves upward during discharging process with little expansion except during phase transition, where it tries to dictate HTF temperature around its melting point. Moreover, the impregnation of PCM capsules between SRS structure helps to improve EDT around its PCT.
(2) The waviness of axial temperature distribution during PCM phase transition was revealed due to the presence of unstable fluid flow structure at the bottom of PCM capsules.
(3) The performance of combined sensible-latent heat TES system is improved by using lower porosities as indicated by the maximum thermocline thickness of 5.19 m, 5.22 m and 5.33 m for a porosity value of 0.4, 0.5 and 0.6, respectively. And it results into enhanced EDE of 96.5%, 86.7% and 79.2% respectively.
(4) Moreover, the results show that with higher fluid inlet velocity thermal energy is discharged quickly during the recovery cycles because of quick solidification of the downstream PCM capsules. Maximum EDT of 307 min with EDE of 96% is observed for u = 0.001 m/s, followed by 166.5 min with 86.7% for u = 0.002 m/s, respectively. While the least is for u = 0.003 m/s with 104.7 min and 81.9%.
(5) The large feature size of SRS affects the thermocline character of combined sensible-latent heat TES negatively as it exhibits the highest W_{tc} of 5.84 m for D_{SRS} = 0.1 m and the least is 4.81 m for D_{SRS} = 0.06 m. Moreover, the results show EDT of 207 min, 167 min and 157 min for feature sizes of 0.06, 0.08 and 0.1 m respectively.

Therefore, a single thermocline TES tank containing cheaper SRS material impregnated with PCM capsules such that majority of it effectively go through phase transition process, is the more viable option. It's a performance optimized TES configuration which bears no concern of thermal ratcheting with stable fluid outlet temperature. However, more investigation is required to harness the maximum potential of the proposed combined sensible-latent heat TES configuration for medium temperature applications. This is the main focus of our next phase of ongoing research in which counter measures for the correct usage of multistage PCM together with SRS will be presented for optimum design.

Acknowledgements

This work was supported by National Natural Science Foundation of China (No. 51536007) and the Foundation for Innovative Research Groups of the National Natural Science Foundation of China (No. 51721004).

References

Abarr, M., Geels, B., Hertzberg, J., Montoya, L.D., 2017. Pumped thermal energy storage and bottoming system part A: concept and model. Energy 120, 320–331. https://doi.org/10.1016/j.energy.2016.11.089.

Abhiji, P., Shi, L., Bielawski, C.W., 2015. A eutectic mixture of galactitol and mannitol as a phase change material for latent heat storage. Energy Convers. Manag. 103, 139–146. https://doi.org/10.1016/j.enconman.2015.06.013.

Ahmed, N., Elfeky, K.E., Wang, Q., 2018. Comparative thermo-economic analysis of structured thermocline combined sensible-latent heat thermal energy storage systems for medium temperature applications. In: 13th Conf. Proc. SDEWES2018.0255.

Alva, G., Liu, L., Huang, X., Fang, G., 2017. Thermal energy storage materials and systems for solar energy applications. Renew. Sustain. Energy Rev. 68, 693–706. https://doi.org/10.1016/j.rser.2016.10.021.

Brosseau, D., Kelton, J.W., Ray, D., Edgar, M., Chisman, K., Emms, B., et al., 2005. Testing of thermocline filler materials and molten-salt heat transfer fluids for thermal energy storage systems in parabolic trough power plants. Trans. ASME-N-Journal Sol. Energy Eng. 127, 109–116.

Dincer, I., Rosen, M., 2002. Thermal Energy Storage: Systems and Applications. John Wiley & Sons.

Elfeky, K.E., Ahmed, N., Wang, Q., 2018. Numerical comparison between single PCM and multi-stage PCM based high temperature thermal energy storage for CSP tower plants. Appl. Therm. Eng. 139, 609–622. https://doi.org/10.1016/j.applthermaleng.2018.04.122.

Felix Regin, A., Solanki, S.C., Saini, J.S., 2009. An analysis of a packed bed latent heat thermal energy storage system using PCM capsules: numerical investigation. Renew. Energy 34, 1765–1773. https://doi.org/10.1016/j.renene.2008.12.012.

Flueckiger, S.M., Yang, Z., Garimella, S.V., 2012. Thermomechanical simulation of the solar one thermocline storage tank. J. Sol. Energy Eng. 134, 041014. https://doi.org/10.1115/1.4007665.

Flueckiger, S.M., Yang, Z., Garimella, S.V., 2013. Review of molten-salt thermocline tank modeling for solar thermal energy storage. Heat Transf. Eng. 34, 787–800.

Galione, P.A., Pérez-Segarra, C.D., Rodríguez, I., Oliva, A., Rigola, J., 2015. Multi-layered solid-PCM thermocline thermal storage concept for CSP plants. Numerical analysis and perspectives. Appl. Energy 142, 337–351. https://doi.org/10.1016/j.apenergy.2014.12.084.

Gasia, J., Miró, L., Cabeza, L.F., 2017. Review on system and materials requirements for high temperature thermal energy storage. Part 1: General requirements. Renew. Sustain. Energy Rev. 75, 1320–1338. https://doi.org/10.1016/j.rser.2016.11.119.

Gil, A., Medrano, M., Martorell, I., Lázaro, A., Dolado, P., Zalba, B., Cabeza, L.F., 2010. State of the art on high temperature thermal energy storage for power generation. Part 1-Concepts, materials and modellization. Renew. Sustain. Energy Rev. 14, 31–55. https://doi.org/10.1016/j.rser.2009.07.035.

Hänchen, M., Brückner, S., Steinfeld, A., 2011. High-temperature thermal storage using a packed bed of rocks – Heat transfer analysis and experimental validation. Appl. Therm. Eng. 31, 1798–1806. https://doi.org/10.1016/j.applthermaleng.2010.10.034.

Jemmal, Y., Zari, N., Maaroufi, M., 2016. Thermophysical and chemical analysis of gneiss rock as low cost candidate material for thermal energy storage in concentrated solar power plants. Sol. Energy Mater. Sol. Cells 157, 377–382. https://doi.org/10.1016/j.solmat.2016.06.002.

Jiménez-Arreola, M., Pili, R., Dal Magro, F., Wieland, C., Rajoo, S., Romagnoli, A., 2018. Thermal power fluctuations in waste heat to power systems: an overview on the challenges and current solutions. Appl. Therm. Eng. 134, 576–584. https://doi.org/10.1016/j.applthermaleng.2018.02.033.

Kim, L.V., 1993. Determination of the heat transfer coefficients in porous media. J. Eng. Phys. Thermophys. 65, 1168–1172. https://doi.org/10.1007/BF00861937.

Kılkış, Ş., Krajačić, G., Duić, N., Rosen, M.A., Al-Nimr, M.A., 2018. Advancements in sustainable development of energy, water and environment systems. Energy Convers. Manag. 176, 164–183. https://doi.org/10.1016/j.enconman.2018.09.015.

Kumaresan, G., Velraj, R., Iniyan, S., 2011. Thermal analysis of D-mannitol for use as phase change material for latent heat storage. J. Appl. Sci. https://doi.org/10.3923/jas.2011.3044.3048.

Libby, C., 2010. Solar thermocline storage systems: preliminary design study. Electr. Power Res. Institute, Palo Alto, CA.

Mat, S., Al-Abidi, A.A., Sopian, K., Sulaiman, M.Y., Mohammad, A.T., 2013. Enhance heat transfer for PCM melting in triplex tube with internal–external fins. Energy Convers. Manag. 74, 223–236.

Meier, A., Winkler, C., Wuillemin, D., 1991. Experiment for modelling high temperature rock bed storage. Sol. Energy Mater. 24, 255–264. https://doi.org/https://doi.org/10.1016/0165-1633(91)90066-T.

Merlin, K., Soto, J., Delaunay, D., Traonvouez, L., 2016. Industrial waste heat recovery using an enhanced conductivity latent heat thermal energy storage. Appl. Energy 183, 491–503. https://doi.org/10.1016/j.apenergy.2016.09.007.

Nallusamy, N., Sampath, S., Velraj, R., 2007. Experimental investigation on a combined sensible and latent heat storage system integrated with constant/varying (solar) heat sources. Renew. Energy 32, 1206–1227. https://doi.org/10.1016/j.renene.2006.04.015.

Pelay, U., Luo, L., Fan, Y., Stitou, D., Rood, M., 2017. Thermal energy storage systems for concentrated solar power plants. Renew. Sustain. Energy Rev. 79, 82–100. https://doi.org/https://doi.org/10.1016/j.rser.2017.03.139.

Qin, F.G.F., Yang, X., Ding, Z., Zuo, Y., Shao, Y., Jiang, R., Yang, X., 2012. Thermocline stability criterions in single-tanks of molten salt thermal energy storage. Appl. Energy 97, 816–821. https://doi.org/10.1016/j.apenergy.2012.02.048.

Schumann, T.E.W., 1929. Heat transfer: a liquid flowing through a porous prism. J. Franklin Inst. 208, 405–416.

Singh, R.P., Kaushik, S.C., Rakshit, D., 2018. Melting phenomena in a finned thermal storage system with graphene nano-plates for medium temperature applications. Energy Convers. Manag. 163, 86–99. https://doi.org/10.1016/j.enconman.2018.02.053.

Strasser, M.N., Selvam, R.P., 2014. A cost and performance comparison of packed bed and structured thermocline thermal energy storage systems. Sol. Energy 108, 390–402. https://doi.org/10.1016/j.solener.2014.07.023.

Tan, F.L., Hosseinizadeh, S.F., Khodadadi, J.M., Fan, L., 2009. Experimental and computational study of constrained melting of phase change materials (PCM) inside a spherical capsule. Int. J. Heat Mass Transf. 52, 3464–3472.

Van Lew, J.T., Li, P., Chan, C.L., Karaki, W., Stephens, J., 2011. Analysis of heat storage and delivery of a thermocline tank having solid filler material. J. Sol. Energy Eng. 133, 021003. https://doi.org/10.1115/1.4003685.

Wakao, N., Kaguei, S., Funazkri, T., 1979. Effect of fluid dispersion coefficients on particle-to-fluid heat transfer coefficients in packed beds. Correlation of Nusselt numbers. Chem. Eng. Sci. 34, 325–336. https://doi.org/10.1016/0009-2509(79)85064-2.

Xu, C., Wang, Z., He, Y., Li, X., Bai, F., 2012. Sensitivity analysis of the numerical study on the thermal performance of a packed-bed molten salt thermocline thermal storage system. Appl. Energy 92, 65–75. https://doi.org/10.1016/j.apenergy.2011.11.002.

Zanganeh, G., Commerford, M., Haselbacher, A., Pedretti, A., Steinfeld, A., 2014. Stabilization of the outflow temperature of a packed-bed thermal energy storage by combining rocks with phase change materials. Appl. Therm. Eng. 70, 316–320. https://doi.org/10.1016/j.applthermaleng.2014.05.020.

Zanganeh, G., Khanna, R., Walser, C., Pedretti, A., Haselbacher, A., Steinfeld, A., 2015. Experimental and numerical investigation of combined sensible-latent heat for thermal energy storage at 575 C and above. Sol. Energy 114, 77–90. https://doi.org/10.1016/j.solener.2015.01.022.